Sub-wavelength gratings in silicon photonic devices for mid-infrared spectroscopy and sensing

Callum J. Stirling[1], Milos Nedeljkovic[1], Colin Mitchell[1], David J. Rowe[1], Goran Z. Mashanovich[1,2]

[1]*Optoelectronics Research Centre, University of Southampton, Southampton, SO17 1BJ, UK*
[2]*School of Electrical Engineering, University of Belgrade, Belgrade, 11120, Serbia*

Abstract

Mid-infrared spectroscopy enabled by silicon photonics has received great interest in recent years as a pathway for a scalable sensing technology. The development of such devices would realise inexpensive and accessible instrumentation for a wide variety of uses over numerous fields. However, not every sensing application is the same; to produce sensors for real-world scenarios, engineers need flexibility in device design but also need to maintain compatibility with scalable fabrication processes. Sub-wavelength gratings can offer a solution to this problem, as they enable the engineering of optical properties using standard fabrication techniques and without requiring new materials. By using sub-wavelength gratings, specific design approaches can be tailored to different applications, such as increasing the interaction of a sensor with an analyte or broadening the bandwidth of an integrated photonic device. Here, we review the development of sub-wavelength grating-based devices for mid-infrared silicon photonics and discuss how they can be exploited for spectroscopic and sensing devices.

Keywords: Silicon photonics, mid-infrared, sub-wavelength grating, sensing, absorption spectroscopy

1. Introduction

The mid-infrared (MIR) wavelength range of 2 - 20 µm offers significant opportunity for specific and sensitive detection and quantification of chemicals across a wide variety of applications. This provides an obvious advantage, for example, in gas sensing where many gases have distinct and strong absorption lines in the MIR. This contrasts with other sensing regimes such as those at near-infrared (NIR) wavelengths, where techniques like overtone spectroscopy and refractometry have comparatively weak absorptions or a lack of innate specificity, respectively. The ability of MIR spectroscopy to distinguish different chemicals within an analyte mixture is critical for real-world scenarios where a variety of substances may be present. In applications with liquid-phase analytes, scenarios with complex mixtures might be the blood analysis of a hospital patient, or monitoring liquid composition for industrial process control.

Integrated photonics has received significant attention and research effort for several decades for use in a variety of applications. In particular, silicon and other group IV materials have proved attractive because they are compatible with complementary metal-oxide-semiconductor (CMOS) fabrication and can therefore take advantage of the mature production infrastructure for microelectronics. Furthermore, the properties of group IV materials mean they have received significant attention for use at MIR wavelengths [1]. Silicon and germanium especially have broad transparencies in the MIR (up to 8 µm and 15 µm respectively) and large refractive indices (approximately 3.4 and 4.0 respectively), so offer the potential for low-loss waveguides and compact devices over a large wavelength range [2, 3]. Alternatively, lower refractive index materials like silicon nitride (index of approximately 2.0) can be used for larger evanescent fields, which can be advantageous for sensing applications [4]. However, this compromises the MIR transparency as silicon nitride is absorbing above 6.7 µm. Various devices have been demonstrated for the MIR range in recent years, across a variety of material platforms, including: low-loss waveguides [5–12], sensing demonstrators [4, 13–16] and spectrometers [17–19].

The challenge for MIR sensing is that conventional instruments are either expensive and restricted to laboratory benchtops, or are specialised and lack the flexibility to sense multiple analytes. For example, a benchtop MIR spectrometer requires costly assembly of multiple components and has moving parts that require calibration, limiting its utility for many applications. By leveraging integrated photonics in silicon and other group IV materials, the functionality of a MIR spectrometer or sensor can be replicated on a "lab-on-a-chip", a small solid-state device that could be produced at low-cost and high-volume using existing CMOS fabrication processes. Consequently, such silicon photonic sensors could be cheap, robust and portable, therefore also accessible and suitable for point-of-need testing, independent of location or access to facilities. Furthermore, silicon photonics can facilitate additional functionality in the device, such as on-chip self-referencing [20] or through established packaging with mi-

crofluidics [21, 22].

As silicon photonic sensors are based on planar stacks of materials, the passive optical behaviour of the waveguides and circuits is typically determined by the inclusion (or removal) of new layers in the stack, or structuring in-plane by patterning with lithography and etching. However, patterning periodic grating structures at a sub-wavelength scale can yield in-plane devices that behave as homogeneous media, with optical properties directly determined by the grating geometry. These sub-wavelength gratings (SWGs) offer more design freedom and can be tailored to provide specific benefits, dependent on the application for the device. Importantly, they offer no additional fabrication complexity over standard waveguide etching.

In this paper, we will review how SWGs have been used to enhance the advantages of silicon photonics for MIR spectroscopy and sensing. In Section 2, we introduce the working principles of SWGs, before outlining the two main approaches for on-chip sensing in the MIR in Section 3. We will then review how the sub-wavelength gratings have been used in each of the two sensing modalities for different benefits in Sections 4 and 5.

2. Sub-wavelength gratings

For a periodic grating with alternating layers of different refractive index material (see Figure 1), the propagation of light perpendicular to the layers (in the k-direction) is determined by the relationship of the grating period, Λ, and the wavelength of the light incident on the grating, λ. When the wavelength is equal to the Bragg wavelength $\lambda_{\text{Bragg}} = 2n_{\text{eff}}\Lambda$, where n_{eff} is the effective index of the Bloch-Floquet mode in the grating, the mode cannot propagate forwards as its frequency is within the photonic bandgap of the grating, and thus the light is completely reflected. In the regime where $\lambda < \lambda_{\text{Bragg}}$, the Bloch-Floquet mode is leaky and light will radiate from the grating as it propagates, while for $\lambda > \lambda_{\text{Bragg}}$ the mode is guided with no reflective or radiative losses [23].

It is this final regime, where the grating becomes an SWG, that provides greater freedom of design. Close to the bandgap, the structure must be considered in full for accurate modelling but at longer wavelengths, $\lambda \gg \Lambda$, the grating can be approximated as an homogeneous material with an anisotropic refractive index tensor $\boldsymbol{n}_{\text{SWG}}$:

$$\boldsymbol{n}^2_{\text{SWG}} = \begin{bmatrix} n^2_{\parallel} & 0 & 0 \\ 0 & n^2_{\parallel} & 0 \\ 0 & 0 & n^2_{\perp} \end{bmatrix}. \tag{1}$$

The index differs for polarisations parallel and perpendicular to the grating interfaces ($n_{\parallel}$ and $n_{\perp}$ respectively), and can be estimated using the Rytov equations [24]:

$$n^2_{\parallel} \approx \frac{a}{\Lambda} n^2_1 + \left(1 - \frac{a}{\Lambda}\right) n^2_2; \tag{2a}$$

$$\frac{1}{n^2_{\perp}} \approx \frac{a}{\Lambda}\frac{1}{n^2_1} + \left(1 - \frac{a}{\Lambda}\right)\frac{1}{n^2_2}, \tag{2b}$$

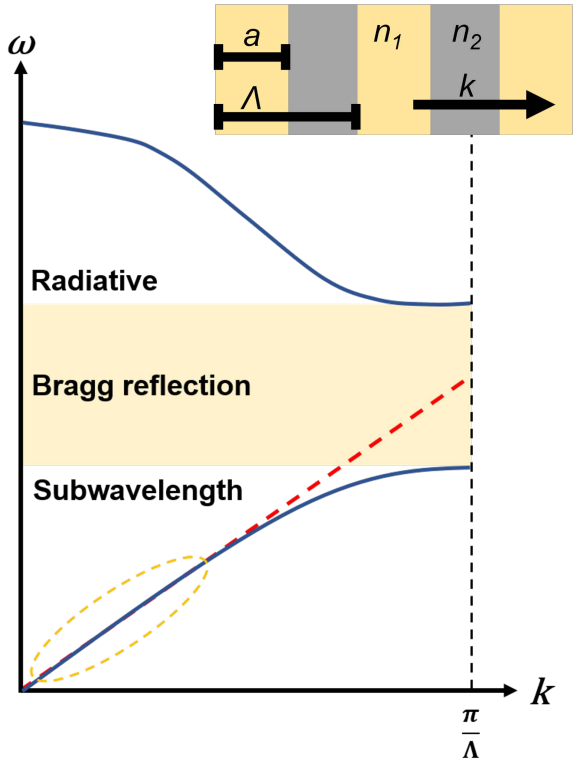

Figure 1: Illustration of the bandstructure of a one-dimensional grating with period Λ. For light propagating with wavevector k, propagating modes at frequency ω are shown in the bandstructure by blue lines. The yellow shaded region indicates the bandgap, with no propagating modes. The red dashed line shows the dispersion for a homogenous waveguide (with n1 = n2), and the region in which the periodic structure can be approximated as homogenous is shown by the dashed orange circle. [inset] Illustration of the grating, consisting of material layers with respective indices n_1 and n_2, and thicknesses a and $\Lambda - a$.

for a grating consisting of materials with indices n_1 and n_2, and with a feature size a (for n_1). Evidently, from Equations 1 and 2, the refractive index of the grating can be tuned between n_1 and n_2 by varying the duty cycle, a/Λ, and period of the grating, enabling far greater range of control of optical behaviour solely from lithographic processes. This characteristic of SWGs which has meant they have found significant usage at NIR wavelengths across a breadth of literature; the reader is referred to previous reviews for implementations of SWG devices in the NIR range [23, 25–27].

Critically for device designers, the feature sizes of the SWG, a and $\Lambda - a$ (for n_1 and n_2 respectively), provide a hard limit on the freedom of the grating design to be readily fabricated using typical modern lithography techniques. Further, as integrated photonic devices move to longer MIR wavelengths, while the grating period can increase comparatively (relaxing the lithographic constraint), thicker waveguiding layers will be required and this provides a different set of fabrication challenges. Features with large aspect ratios are difficult to fabricate with a uniform etch profile and factors such as aspect ratio-

dependent etching have non-negligible effects [28]. SWGs are particularly sensitive to fabrication errors from under-etched material within the grating and, as a consequence, can quickly deviate from their designed performance. To date, SWG devices have not been demonstrated (to the authors' knowledge) on germanium layers thicker than 1 µm in integrated photonic circuits [29].

3. Sensing systems

To achieve absorption spectroscopy on a silicon photonic chip, there are broadly two approaches that can be taken. The first method is to use a narrowband laser that can be tuned over an absorption feature of the analyte, or multiple features if spectrally close. For example, a quantum cascade laser can be tuned over a range sufficient to resolve a gas absorption line [30], as can distributed feedback lasers [31]. Broader tuning of a laser is possible using on-chip external cavities [32]. Techniques such as wavelength modulation spectroscopy can even increase the sensitivity of the device through tuning of the input source [33, 34].

As illustrated in Figure 2, the tunable source is coupled into a chip and the optical power is split equally into two paths. One of these acts as a real-time reference to account for variation of input power, which may be induced while tuning, or alternatively due to fabrication or alignment stability. The other path is exposed to the analyte, such that the evanescent field of the waveguide mode interacts with the analyte and results in a wavelength-dependent absorption as the source wavelength is swept. The source itself can be external with a coupling mechanism (such as free-space, fibre, or interconnect) or integrated on the chip, in either a monolithic [35] or hybrid [36] system. By measuring the transmission through the sensing arm and normalising to the reference arm, to remove any losses not induced by the analyte, the absorption spectrum for the analyte can be recovered.

The approach illustrated in Figure 2 is particularly appropriate for gas sensing as gases have strong and narrow absorption features. Typically, the relative concentrations for gas sensing in many use cases are very small because trace amounts are being measured against the atmospheric background. For example, in monitoring of the three predominant environmental greenhouse gases, the global average atmospheric concentrations of carbon dioxide, methane and nitrous oxide are 417 ppm (August 2023), 1.9 ppm (July 2023) and 0.3 ppm (July 2023) respectively [37]. Despite the strong absorption lines, the low concentrations means that the sensitivity of the system must be maximised. The general focus from a device design perspective is then to maximise the light-analyte interaction in the system, which can be achieved by increasing the optical path length that is exposed to the analyte, or the fraction of light in the waveguide that overlaps with the analyte, or both. Put differently, we require waveguides to have a minimal propagation loss, α, and a

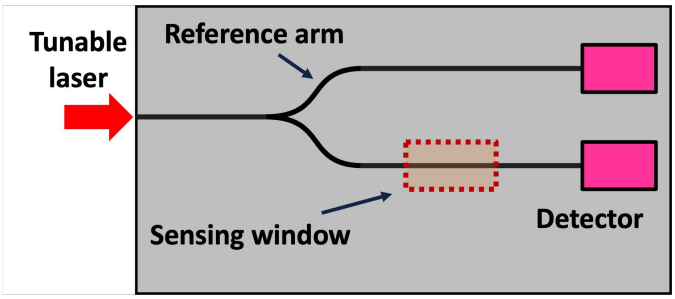

Figure 2: Illustration of a simple chip for narrowband tunable laser absorption spectroscopy.

maximal modal confinement in the analyte, Γ [38], for the greatest fractional change in optical power ΔP [39]:

$$\begin{aligned}\Delta P &= \exp(-\alpha L)\cdot[1-\exp(-\Gamma\alpha' L)] \\ &\approx \exp(-\alpha L)\cdot\Gamma\alpha' L\end{aligned} \tag{3}$$

where α' is the loss per unit length caused by the analyte. Notably, in a high-index waveguide the material dispersion has be accounted for when calculating Γ (assuming propagation of light in the z-direction) [40]:

$$\Gamma = \frac{n_{\mathrm{g}}}{\mathrm{Re}\{n_{\mathrm{cl}}\}}\frac{\iint_{\mathrm{cl}}\varepsilon|\mathbf{E}|^2dxdy}{\iint_{-\infty}^{\infty}\varepsilon|\mathbf{E}|^2dxdy} \tag{4}$$

where n_{g} is the group index of the waveguide mode, n_{cl} is the refractive index of the cladding, ε is the permittivity and $\mathbf{E}$ is the electric field.

Various waveguides have been proposed to maximise the external modal confinement such as slot waveguides, where the light is confined to a channel in the centre of the waveguide [41–44], or membrane waveguides, that allow access to the evanescent mode both above and below the waveguide [15, 45, 46]. However, these designs typically have drawbacks such as high-propagation losses or complex fabrication with restrictive tolerances, which limits their scalability.

In the second approach, rather than using a single wavelength, a broadband source is coupled into the circuit. The interaction between the light and the analyte could occur on or off-chip, as it may be advantageous in some scenarios to not risk contamination of the device, such as when processing biological samples, but to still miniaturise the overall instrument. In both configurations, the photonic circuit would be used to reconstruct the absorption spectrum through either: (a) Fourier-transform infrared (FTIR) spectroscopy; or, (b) MIR dual-comb spectroscopy [47, 48]. For this discussion, we will focus on FTIR spectroscopy but the considerations paid to the broadband operation of the circuit components are applicable to either case.

While the thermal sources typically used in FTIR spectroscopy cannot be coupled efficiently into a waveguide, other options for broad MIR sources could include arrays

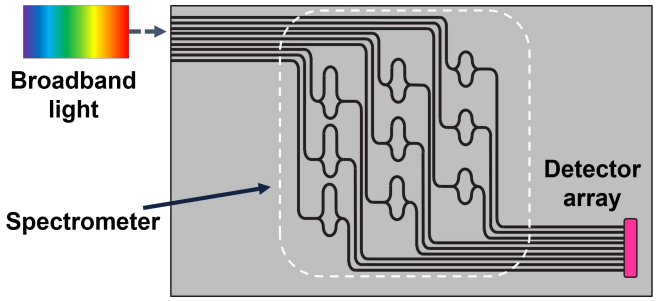

Figure 3: FTIR spectrometer with fixed delay lines, with light-analyte interaction off-chip.

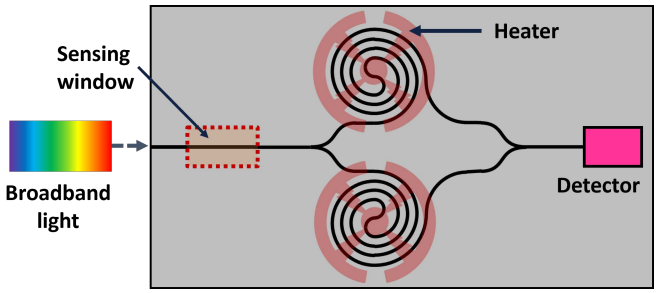

Figure 4: FTIR spectrometer with tunable delay lines, and on-chip light-analyte interaction.

of quantum cascade lasers [49], supercontinuum generation [50–52] or on-chip broadband emitters [53]. Following the light-analyte interaction, the light is passed to the spectrometer, such as those illustrated: an array of Mach-Zehnder interferometers (MZIs) with fixed path delays (Figure 3), such as [17], or a single MZI with a tunable delay from on-chip heaters (Figure 4), as in [18]. Both circuits are required to operate over a large spectral range and therefore the individual circuit components (including waveguides) must also have a broad working bandwidth. These devices would be used where the application necessitates analysis of multiple features in the absorption spectrum and thus it is a requirement to not have strong wavelength-dependent spectral features from the circuit. Multimode waveguides, while having been used for broadband sensing demonstrations [54], would cause such wavelength-dependent features due to the beating as the different supported modes interfere and may result in wavelength-dependent errors in the power spectral density measurement, limiting the FTIR sensitivity and resolution.

However, designing a silicon photonic waveguide to be single-mode over a large wavelength range is inherently more challenging than for a narrow optical band. For a rib or strip waveguide of a fixed geometry, towards shorter wavelengths the waveguide becomes multimoded, while at longer wavelengths the fundamental mode is cut off. Material platforms like SiGe have relied on the dispersion inherent to the material to expand the bandwidth of the waveguide and other devices (including splitters and interferometers) [55, 56], but this the approach is not applicable to rib or strip waveguides in other platforms.

4. Devices for narrowband circuits

Within narrowband gas sensing applications, SWGs can provide much needed flexibility to realise novel waveguide designs. As discussed in the previous section, the focus here is to maximise modal overlap with the analyte, Γ, without increasing (or even reducing) the waveguide loss, α.

Suspending waveguides, in both silicon and germanium, by removing of the underlying cladding allows the full transparency range of the waveguiding layer to be exploited. For example, the silicon dioxide layer in silicon-on-insulator (SOI) starts absorbing for $\lambda > 4$ µm and the waveguide mode will have a non-negligible evanescent field that overlaps with it, thereby increasing α. For suspended waveguides, this absorption by the cladding material is avoided by simply removing the cladding. For gas sensing, this provides the additional advantage that the analyte can access the evanescent field on both sides of the waveguiding layer.

The waveguides are suspended by locally underetching using a wet chemical or vapour etch to remove the lower cladding, typically silicon dioxide removed using hydrofluoric acid. Vias between the surface and cladding are required to provide access to the etchant and, for some designs, the waveguide and the vias are defined with separate lithography and etch steps [12, 15, 57].

An alternate approach is to use an SWG cladding for suspended waveguides, similar to that shown in Figure 5. In the SWG, the holes are fully etched to reach the underlying layers, with strips of the waveguiding layer spanning the gap between the membrane waveguide and the unetched regions to form the rest of the grating. This means that the holes can act as the vias and, because the holes are also used to define the waveguide, this significantly simplifies fabrication to a single lithography and etch step. Moreover, the vias are immediately adjacent to the waveguide and so it is more straightforward to obtain uniform removal of the cladding underneath the waveguide, which can otherwise cause reflections, scattering or absorption.

Suspended waveguides with SWG claddings have been demonstrated in both silicon and germanium with low propagation losses: for suspended silicon, $\alpha = 0.82$ dB/cm and 3.1 dB/cm for $\lambda = 3.8$ µm and 7.67 µm respectively [58, 59]; for suspended germanium, $\alpha = 5.3$ dB/cm at $\lambda = 7.7$ µm [29]. Note that the longer wavelength demonstration for suspended silicon [59] required a silicon layer thickness of 1.4 µm, rather than 500 nm in [58], to prevent substantial vertical power leakage to the substrate. Hybrid SWG-clad slot waveguides have also been demonstrated, to increase Γ: $\alpha = 2.8$ dB/cm at $\lambda = 2.25$ µm [60]. SWG-clad suspended silicon waveguides have also been used for demonstrations of gas sensing at $\lambda = 6.65$ µm [16] and to build an FTIR spectrometer for $\lambda \sim 5.5$ µm [61].

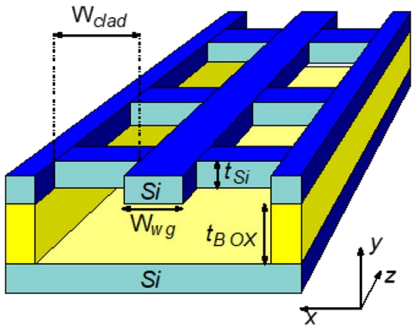

Figure 5: Illustration of the suspended silicon waveguide (width W_{wg} and thickness t_{Si}) with SWG cladding (width W_{clad}), in which light propagates in the z-direction. The underlying silicon dioxide cladding (thickness t_{BOX}) has been removed.

The confinement of the modes for the SWG-clad waveguides comes from the refractive index contrast between the waveguide material (n_{Si} or n_{Ge}) and $\boldsymbol{n}_{\mathrm{SWG}}$. Like the grating holes that act as etchant vias, the strips in the SWG also serve a dual purpose and provide support for the central core. Consequently, there are three main considerations when designing these waveguides [29].

1. Mechanical stability: are the strips thick enough to be mechanically robust?
2. Fabrication: can the etchant flow through the holes? Are the features smaller than lithography allows?
3. Optical properties: does the period of the cladding satisfy the SWG condition? Is the waveguide single-moded?

The flexibility afforded by the SWG geometry allows all three criteria to be satisfied to some degree, with a level of compromise between them [62]. Notably, the suspended silicon waveguides using SWG cladding can be produced using deep-ultraviolet lithography as part of a multi-project-wafer service and, for example, is offered as a platform by CORNERSTONE (a research-aligned rapid prototyping facility) [63].

The all-dielectric metamaterial-comb (ADMAC) waveguide of Liu *et al.* (Figure 6) is a similarly suspended design but with a very different structure [64]. For this waveguide, both the waveguide core and the cladding consist of an SWG. Using an interdigitated comb structure, where silicon strips extend to interlock at the centre, light is guided in the region where the interlocking features overlap. Lateral confinement is provided by the non-overlapping regions that have a different duty cycle than the core region. While the loss of the ADMAC waveguide is larger than SWG-clad waveguides (4.7 dB/cm at $\lambda = 7.33$ µm) it achieves $\Gamma = 113\%$ (i.e. better than free space) due to the waveguide dispersion. Compared to other suspended silicon waveguides with lower propagation loss, such as free-standing waveguides ($\lambda = 4.24$ µm, $\Gamma = 44\%$, $\alpha = 3$ dB/cm) [46] or those with SWG claddings ($\lambda = 6.65$ µm, $\Gamma = 24.3\%$, $\alpha = 3.9$ dB/cm) [16], this gives over a two- or

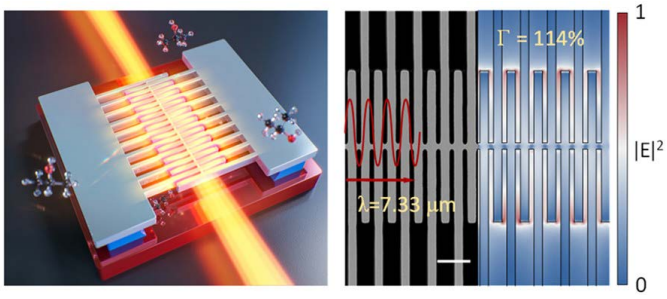

Figure 6: Illustration of the ADMAC waveguide, reproduced from [64].

threefold improvement in performance using the figure-of-merit defined by Kita *et al.*, Γ/α [38].

Suspended waveguides using SWGs have also enabled other devices required for the circuit in Figure 2. Bolometers are photodetectors in which incident light is absorbed, causing a local temperature change which, in turn, results in a measurable change in electrical resistance across the detector. Despite having worse performance than other cooled detectors, their room-temperature operation and CMOS-compatibility have made them the dominant technology in commercial MIR cameras [65]. In [66], integrated bolometers were fabricated on suspended silicon waveguides to decrease the heat loss to the substrate and thus increase the detector sensitivity (from 0.80%/mW to 1.1%/mW at $\lambda = 3.8$ µm, and up to 24.6%/mW in later generations by changing from crystalline to amorphous silicon [67]): the fabricated device is shown in Figure 7. The bolometer includes a gold antenna to act as a plasmonic absorber, to confine the light locally and increase the absorption efficiency of the device. However, this also reduces the absorption bandwidth: a simulated 3-dB bandwidth of 640 nm in [66], and an experimentally-derived 3-dB bandwidth of 160 nm in [67]. For narrowband sensing applications, in which only small sections of an absorption spectrum would be required, this is more than sufficient. The SWG-waveguide was useful in the suspended design to reduce the number of fabrication steps required to make the bolometer and thereby minimising the cost of manufacture, which is a key advantage for the device.

If the detector or source is not integrated on-chip, some form of optical input and output is needed. For narrowband sensing circuits, grating couplers are often preferred because they avoid the optical-quality preparation of waveguide facets and have relaxed alignment tolerances compared to end-fire coupling [68]. A conventional grating coupler is defined by etched strips, but these areas can be replaced with an SWG to make a two-dimensional grating. As already shown, this provides tunability over the refractive index and consequently increased design flexibility. Using this approach, SWG grating couplers have been demonstrated with increased coupling efficiency, optical bandwidth and reduced back reflections in a variety of material platforms, including: SOI at $\lambda = 3.7$ µm [69];

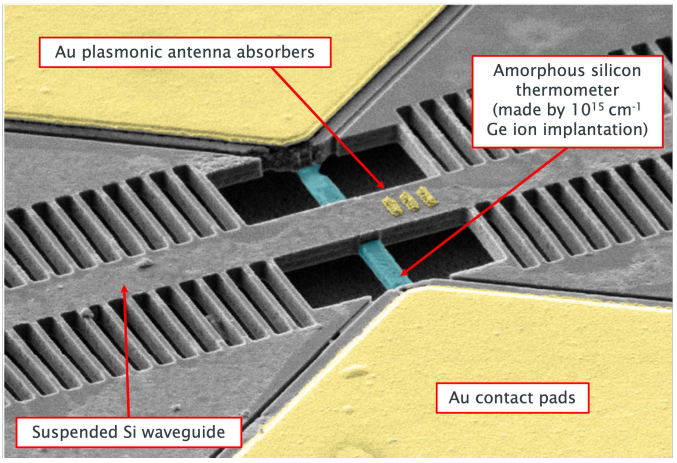

Figure 7: SEM image of the bolometer based on the suspended waveguide with SWG cladding, reproduced from [66].

silicon-on-sapphire at $\lambda = 2.75$ µm [70]; suspended silicon at $\lambda = 2.75$ µm [71]; and suspended germanium at $\lambda = 2.37$ µm [72].

5. Devices for broadband circuits

For liquid-phase applications, maximising Γ is not necessarily optimal as it may introduce a large system loss from the environment. This is particularly important for aqueous samples such as most biofluids; water is heavily absorbing across the MIR wavelength range. Rather, the challenge is to optimise the optical bandwidth to measure multiple features in the analyte absorption spectrum and thereby distinguish a range of molecules present within the specific context. Using healthcare applications as an example, this might include multivariate chemometric analysis for cancer diagnosis [73] or measurement of pharmacological molecules with a blood sample [74]. One of the fundamental challenges is the availability of waveguides that can have both low loss across the entire bandwidth required and only support the fundamental mode, to avoid wavelength-dependent transmission errors in the circuit.

The endlessly single-mode (ESM) waveguide, shown in Figure 8, consists of a rib waveguide in which the lateral cladding has been replaced with a two-dimensional grating to maintain single-mode propagation beyond a conventional rib or strip [75]. In the direction parallel to the propagation within the waveguide core, the grating period is chosen such that, at the shortest operable wavelength, the grating is in the sub-wavelength regime and is thus an SWG. Consequently, in the direction perpendicular to the core, the cladding behaves as a one-dimensional grating with alternating layers $\boldsymbol{n}_{\mathrm{SWG}}$ and n_{Si}. In this case, it is the inherent tunability of $\boldsymbol{n}_{\mathrm{SWG}}$ that allows the waveguide to be tailored so that the fundamental mode can expand, avoiding the long wavelength cut-off, because the contrast between the core and the cladding is reduced. Likewise, it can maintain the leakiness of higher-order modes into the

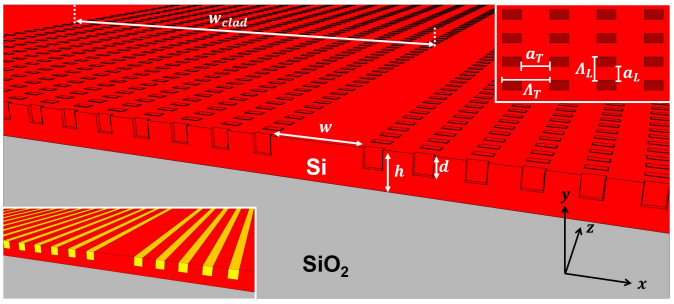

Figure 8: Illustration of the ESM waveguide, reproduced from [76]. [top] Top-view of the waveguide. [bottom] SWG regions of the waveguide cladding.

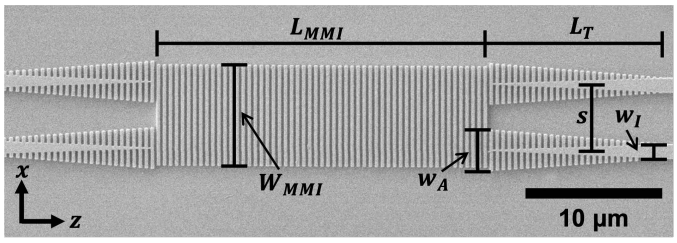

Figure 9: SEM image of the SWG-MMI for MIR wavelengths, reproduced from [79].

cladding as they will overlap with the regions of $\boldsymbol{n}_{\mathrm{SWG}}$ to a greater degree than the fundamental mode; the combination of these effects meant that single-mode propagation was achieved over an octave of frequency in the MIR ($\lambda =$ 2 - 3.8 µm) with $\alpha \sim 1.5$ dB/cm [76].

Other devices utilise SWGs more than just for a tunable refractive index however; the birefringence of $\boldsymbol{n}_{\mathrm{SWG}}$ has also been effectively exploited [26]. In particular, the central multimode waveguide in a multimode interferometer (MMI) has been replaced with an SWG (see Figure 9). First demonstrated at NIR wavelengths [77], the SWG-MMI design takes advantage of the anisotropic refractive index and dispersion properties of the SWG [78] to both reduce the footprint of an MMI and increase the optical bandwidth, doubling it compared to a conventional design for the MIR version: a bandwidth $\Delta\lambda > 600$ nm within the range $\lambda = 3$ - 4 µm [79]. Likewise, SWGs have been combined with other integrated beamsplitters such as polarisation splitters, $\Delta\lambda = 50$ nm around $\lambda = 2.5$ µm [80], or directional couplers, $\Delta\lambda = 175$ nm around $\lambda = 3.8$ µm [81], for the MIR wavelength range. Within the broadband sensing circuit, splitters are crucial for making devices like spectrometers, or even simply enabling basic functionality such as coupling light into both the sensing and reference arms.

Other devices, in particular those with non-linear behaviours, also benefit from dispersion control in the waveguides. As discussed earlier, waveguide-based supercontinuum generation is a potential option for on-chip broadband sources but such waveguides are required to have near-uniform dispersion profiles with respect to wavelength [50–

52]. The customisable nature of the SWG means that the waveguide dispersion can be directly engineered through the SWG geometry. Strip waveguides with either a solid core and SWG cladding [82, 83] or simply an SWG core [84] have been designed for this purpose. In both cases, the design lead to flattened dispersion profiles over much of the SOI transparency range ($\lambda \sim 1.1$ - 4 µm), covering both NIR and MIR wavelengths.

6. Conclusions

Within MIR sensing and on-chip spectroscopy, there are several ways in which SWGs offer great functionality. For gas sensing and other narrowband applications, they offer a route to maximising the interaction between a sensor and an analyte, while maintaining low propagation losses and with a minimally complex fabrication scheme. Whilst other approaches have addressed one or more of the goals, waveguides using SWGs are unique in that they have achieved all three. For applications that require operation over a broader wavelength range, SWGs offer unparalleled utility. The ability to customise waveguide dispersion, isolate the fundamental mode or tailor the optical bandwidth of a photonic circuit all result in practical benefits for a sensor designer.

However, there are still areas for further development. The small feature sizes for SWGs are typically realised using electron beam lithography, which inherently has a low throughput. Achieving the required resolution can be challenging for more scalable techniques and this restricts the freedom of design for the SWG. However, recent developments within scalable lithography may mitigate this. For example, immersion lithography, which can achieve feature sizes down to 40 nm [85], has been used to realise SWG-based 2×2 MMIs at NIR wavelengths with 75 nm feature sizes [86]. While this limitation reduces with increasing wavelength, the thicker waveguiding layers needed for the long-wave MIR range offers a different restraint. The larger etch aspect ratios required for defining SWG features in thick layers remains a concern and, consequently, whether SWGs will be effective at wavelengths beyond 8 µm remains to be seen.

Acknowledgments

The authors gratefully acknowledge funding from the Engineering and Physical Science Research Council (EP/V047663/1, EP/L021129/1, EP/N00762X/1, EP/L01162X/1, EP/W020254/1) and the Royal Academy of Engineering (RF201617/16/33).

References

[1] G. Z. Mashanovich, M. Nedeljkovic, J. Soler-Penades, Z. Qu, W. Cao, A. Osman, Y. Wu, C. J. Stirling, Y. Qi, Y. X. Cheng, L. Reid, C. G. Littlejohns, J. Kang, Z. Zhao, M. Takenaka, T. Li, Z. Zhou, F. Y. Gardes, D. J. Thomson, and G. T. Reed. Group IV mid-infrared photonics [Invited]. *Opt. Mater. Express*, 8(8):2276–2286, 2018.

[2] R. Soref. Mid-infrared photonics in silicon and germanium. *Nat. Photonics*, 4:495–497, 2010.

[3] J.-M. Fedeli and S. Nicoletti. Mid-infrared Mid-IR silicon-based photonics. *Proc. IEEE*, 106(12):2302–2312, 2018.

[4] J. Zhou, D. Al Husseini, J. Li, Z. Lin, S. Sukhishvili, G. L. Coté, R. Gutierrez-Osuna, and P. T. Lin. Detection of volatile organic compounds using mid-infrared silicon nitride waveguides sensors. *Sci. Reports*, 12(5572), 2022.

[5] F. Li, S. D. Jackson, C. Grillet, E. Magi, D. Hudson, S. J. Madden, Y. Moghe, C. O'Brien, A. Read, S. G. Duvall, P. Atanackovic, B. J. Eggleton, and D. J. Moss. Low propagation loss silicon-on-sapphire waveguides for the mid-infrared. *Opt. Express*, 19(16):15212–15220, 2011.

[6] S. Khan, J. Chiles, J. Ma, and S. Fathpour. Silicon-on-nitride waveguides for mid- and near-infrared integrated photonics. *Appl. Phys. Lett.*, 102(12):121104, 2013.

[7] G. Z. Mashanovich, F. Y. Gardes, D. J. Thomson, Y. Hu, K. Li, M. Nedeljkovic, J. Soler Penadés, A. Z. Khokhar, C. J. Mitchell, S. Stankovic, R. Topley, S. A. Reynolds, Y. Wang, B. Troia, V. M. N. Passaro, C. G. Littlejohns, T. Dominguez Bucio, P. R. Wilson, and G. T. Reed. Silicon photonic waveguides and devices for near- and mid-IR applications. *IEEE J. Sel. Top. Quantum Electron.*, 21(4):407–418, 2015.

[8] L. He, Y. Guo, Z. Han, K. Wada, L. C. Kimerling, J. Michel, A. M. Agarwal, G. Li, and L. Zhang. Loss reduction of silicon-on-insulator waveguides for deep mid-infrared applications. *Opt. Lett.*, 42(17):3454–3457, 2017.

[9] M. Montesinos-Ballester, V. Vakarin, Q. Liu, X. Le Roux, J. Frigerio, A. Ballabio, A. Barzaghi, C. Alonso-Ramos, L. Vivien, G. Isella, and D. Marris-Morini. Ge-rich graded SiGe waveguides and interferometers from 5 to 11 µm wavelength range. *Opt. Express*, 28(9):12771–12779, 2020.

[10] K. Gallacher, R. W. Millar, U. Griškevičiūte, L. Baldassarre, M. Sorel, M. Ortolani, and D. J. Paul. Low loss Ge-on-Si waveguides operating in the 8-14 µm atmospheric transmission window. *Opt. Express*, 26(20):25667–25675, 2018.

[11] D. A. Kozak, T. H. Stievater, R. Mahon, and W. S. Rabinovich. Germanium-on-silicon waveguides at wavelengths from 6.85 to 11.25 microns. *IEEE J. Sel. Top. Quantum Electron.*, 24(6), 2018.

[12] A. Osman, M. Nedeljkovic, J. Soler Penadés, Y. Wu, Z. Qu, A. Z. Khokhar, K. Debnath, and G. Z. Mashanovich. Suspended low-loss germanium waveguides for the longwave infrared. *Opt. Lett.*, 43(24):5997–6000, 2018.

[13] D. Grassani, E. Tagkoudi, H. Guo, C. Herkommer, F. Yang, T. J. Kippenberg, and C.-S. Brès. Mid infrared gas spectroscopy using efficient fiber laser driven photonic chip-based supercontinuum. *Nat. Commun.*, 10(1553), 2019.

[14] N. Teigell Benéitez, B. Baumgartner, J. Missinne, S. Radosavljevic, D. Wacht, S. Hugger, P. Leszcz, B. Lendl, and G. Roelkens. Mid-IR sensing platform for trace analysis in aqueous solutions based on a germanium-on-silicon waveguide chip with a mesoporous silica coating for analyte enrichment. *Opt. Express*, 28(18):27013–27027, 2020.

[15] M. Vlk, A. Datta, S. Alberti, H. D. Yallew, V. Mittal, G. S. Murugan, and J. Jagerska. Extraordinary evanescent field confinement waveguide sensor for mid-infrared trace gas spectroscopy. *Light. Sci. & Appl.*, 10(26), 2021.

[16] W. Liu, Y. Ma, Y. Chang, B. Dong, J. Wei, Z. Ren, and C. Lee. Suspended silicon waveguide platform with subwavelength grating metamaterial cladding for long-wave infrared sensing applications. *Nanophotonics*, 10(7):1861–1870, 2021.

[17] M. Nedeljkovic, A. V. Velasco, A. Z. Khokhar, A. Delâge, P. Cheben, and G. Z. Mashanovich. Mid-infrared silicon-on-insulator Fourier-transform spectrometer chip. *IEEE Photonics Technol. Lett.*, 28(4):528–531, 2016.

[18] M. C. M. M. Souza, A. Grieco, N. C. Frateschi, and Y. Fainman. Fourier transform spectrometer on silicon with thermo-optic non-linearity and dispersion correction. *Nat. Commun.*,

9(665), 2018.

[19] A. Vasiliev, M. Muneeb, J. Allaert, J. Van Campenhout, R. Baets, and G. Roelkens. Integrated silicon-on-insulator spectrometer with single pixel readout for mid-infrared spectroscopy. *IEEE J. Sel. Top. Quantum Electron.*, 24(6), 2018.

[20] Y. Qi, Z. Zheng, M. Banakar, Y. Wu, A. Gangnaik, D. J. Rowe, V. Mittal, J. Butement, J. S. Wilkinson, G. Z. Mashanovich, and M. Nedeljkovic. Integrated switching circuit for low-noise self-referenced mid-infrared absorption sensing using silicon waveguides. *IEEE Photonics J.*, 13(6), 2021.

[21] P. Wägli, Y.-C. Chang, A. Homsy, L. Hvozdara, H. P. Herzig, and N. F. de Rooij. Microfluidic droplet-based liquid-liquid extraction and on-chip IR spectroscopy detection of cocaine in human saliva. *Anal. Chem.*, 85:7558–7565, 2013.

[22] C. Dhote, A. Singh, and S. Kumar. Silicon photonics sensors for biophotonic applications - a review. *IEEE Sensors J.*, 22(19):18228–18239, 2022.

[23] P. Cheben, R. Halir, J. H. Schmid, H. A. Atwater, and D. R. Smith. Subwavelength integrated photonics. *Nature*, 560:565–572, 2018.

[24] S. M. Rytov. Electromagnetic properties of a finely stratified medium. *Soviet Phys. JETP*, 2:466–475, 1956.

[25] R. Halir, A. Ortega-Moñux, D. Benedikovic, G. Z. Mashanovich, J. G. Wangüemert-Pérez, J. H. Schmid, Í. Molina-Fernández, and P. Cheben. Subwavelength-grating metamaterial structures for silicon photoics devices. *Proc. IEEE*, 106(12):2144–2157, 2018.

[26] J. M. Luque-González, A. Sánchez-Postigo, A. Hadij-ElHouati, A. Ortega-Moñux, J. G. Wangüemert-Pérez, J. H. Schmid, P. Cheben, Í. Molína-Fernández, and R. Halir. A review of silicon subwavelength gratings: building break-through devices with anisotropic materials. *Nanophotonics*, 10(11):2765–2797, 2021.

[27] N. L. Kazanskiy, M. A. Butt, and S. N. Khonina. Silicon photonic devices realized on refractive index engineered sub-wavlength grating waveguides - A review. *Opt. & Laser Technol.*, 138:106863, 2021.

[28] L. Meng, J. Li, C. Zhao, and J. Yan. Aspect ratio dependent analytic model and application in deep silicon etch. *ECS Solid State Lett.*, 3(5), 2014.

[29] A. Sánchez-Postigo, A. Ortega-Moñux, J. Soler Penadés, A. Osman, M. Nedeljkovic, Z. Qu, Y. Wu, Í. Molína-Fernández, P. Cheben, G. Z. Mashanovich, and J. G. Wangüemert-Pérez. Suspended germanium waveguides with subwavelength-grating metamaterial cladding for the mid-infrared band. *Opt. Express*, 29(11), 2021.

[30] A. Bismuto, Y. Bidaux, C. Tardy, R. Terazzi, T. Gresch, J. Wolf, S. Blaser, A. Muller, and J. Faist. Extended tuning of mid-IR quantum cascade lasers using integrated resistive heaters. *Opt. Express*, 23(23):29715–29722, 2015.

[31] L. Tombez, E. J. Zhang, J. S. Orcutt, S. Kamlapurkar, and W. M. J. Green. Methane absorption spectroscopy on a silicon photonic chip. *Optica*, 4(11):1322–1325, 2017.

[32] T. Komljenovic, S. Srinivasan, E. Norberg, M. Davenport, G. Fish, and J. E. Bowers. Widely tunable narrow-linewidth monolithically integrated external-cavity semiconductor lasers. *IEEE J. Sel. Top. Quantum Electron.*, 21(6), 2015.

[33] G. B. Rieker, J. B. Jeffries, and R. K. Hanson. Calibration-free wavelength-modulation spectroscopy for measurements of gas temperature and concentration in harsh environments. *Appl. Opt.*, 48(29):5546–5560, 2009.

[34] H. Zhao, C. Zheng, M. Pi, L. Liang, F. Song, Y. Zhang, Y. Wang, and F. K. Tittel. On-chip mid-infrared silicon-on-insulator waveguide methane sensor using two measurement schemes at 3.291 µm. *Front. Chem.*, 10, 2022.

[35] E. Tournié, L. Monge Bartolome, M. Rio Calvo, Z. Loghmari, D. A. Díaz-Thomas, R. Teissier, A. N. Baranov, L. Cerutti, and J.-B. Rodriguez. Mid-infrared III-V semiconductor lasers epitaxially grown on si substrates. *Light. Sci. & Appl.*, 11(165), 2022.

[36] A. Spott, E. J. Stanton, N. Volet, J. D. Peters, J. R. Meyer, and J. E. Bowers. Heterogenous integration for mid-infrared silicon photonics. *IEEE J. Sel. Top. Quantum Electron.*, 23(6), 2017.

[37] National Oceanic and Atmospheric Administration (NOAA). Global monitoring laboratory - carbon cycle greenhouse gases. https://gml.noaa.gov/ccgg/trends/ Accessed: 9 November 2023.

[38] D. M. Kita, J. Michon, S. G. Johnson, and J. Hu. Are slot and sub-wavlength grating waveguides better than strip waveguides for sensing? *Optica*, 5(9):1046–1054, 2018.

[39] H. T. Lin, Z. Q. Luo, T. Gu, L. C. Kimerling, K. Wada, A. Agarwal, and J. J. Hu. Mid-infrared integrated photonics on silicon: a perspective. *Nanophotonics*, 7(2):393–420, 2018.

[40] J. T. Robinson, K. Preston, O. Painter, and M. Lipson. First-principle derivation of gain in high-index-contrast waveguides. *Opt. Express*, 16(21):16659–16669, 2008.

[41] Y. Zou, H. Subbaraman, S. Chakravarty, X. Xu, A. Hosseini, W.-C. Lai, P. Wray, and R. T. Chen. Grating-coupled silicon-on-sapphire integrated slot waveguides opertating at mid-infrared wavelengths. *Opt. Lett.*, 39(10):3070–3073, 2014.

[42] J. Soler Penadés, A. Z. Khokhar, M. Nedeljkovic, and G. Z. Mashanovich. Low-loss mid-infrared SOI waveguides. *IEEE Photonics Technol. Lett.*, 27(11):1197–1199, 2015.

[43] B. Kumari, A. Barh, R. K. Varshney, and B. P. Pal. Silicon-on-nitride slot waveguide: A promising platform as mid-IR trace gas sensor. *Sensors Actuators B: Chem.*, 236:759–764, 2016.

[44] J. Lim, J. Shim, D.-M. Geum, and S. Kim. Experimental demonstration of Germanium-on-Silicon slot waveguides at mid-infrared wavelength. *IEEE Photonics J.*, 14(3), 2022.

[45] C. Ranacher, C. Consani, A. Tortschanoff, R. Jannesari, M. Bergmeister, T. Grille, and B. Jakoby. Mid-infrared absorption gas sesning using a silicon strip waveguide. *Sensors Actuators A: Phys.*, 277:117–123, 2018.

[46] F. Ottonello-Briano, C. Errando-Herranz, H. Rödjegård, H. Martin, H. Sohlström, and K. B. Gylfason. Carbon dioxide absorption spectroscopy with a mid-infrared silicon photonic waveguide. *Opt. Lett.*, 45(1):109–112, 2020.

[47] N. Nader, D. L. Maser, F. C. Cruz, A. Kowligy, H. Timmers, J. Chiles, C. Fredrick, S. W. Nam D. A. Westly, R. P. Mirin, J. M. Shainline, and S. Diddams. Versatile silicon-waveguide supercontinuum for coherent mid-infrared spectroscopy. *APL Photonics*, 3(3):036102, 2018.

[48] M. Yu, Y. Okawachi, A. G. Griffith, N. Picqé, M. Lipson, and A. L. Gaeta. Silicon-chip-based mid-infrared dual-comb spectroscopy. *Nat. Commun.*, 9(1869), 2018.

[49] W. Zhou, N. Bandyopadhyay, D. Wu, R. McClintock, and M. Razeghi. Monolithically, widely tunable quantum cascade lasers based on a heterogeneous active region design. *Sci. Reports*, 6(25213), 2016.

[50] N. Singh, D. D. Hudson, and B. J. Eggleton. Silicon-on-sapphire pillar waveguides for Mid-IR supercontinuum generation. *Opt. Express*, 23(13):17345–17354, 2015.

[51] M. Yang, Y. Guo, J. Wang, Z. Han, K. Wada, L. C. Kimerling, A. M. Agarwal, J. Michel, G. Li, and L. Zhang. Mid-IR supercontinuum generated in low-dispersion Ge-on-Si waveguides pumped by sub-ps pulses. *Opt. Express*, 25(14):16116–16122, 2017.

[52] M. R. Karim, H. Ahmad, S. Ghosh, and B. M. A. Rahman. Design of dispersion-engineered As_2Se_3 channel waveguide for mid-infrared region supercontinuum generation. *J. Appl. Phys.*, 123(21):213101, 2018.

[53] C.-C. Hou, H.-M. Chen, J.-C. Zhang, N. Zhuo, Y.-Q. Huang, R. A. Hogg, D. T. D. Childs, J.-Q. Ning, Z.-G. Wang, F.-Q. Liu, and Z.-Y. Zhang. Near-infrared and mid-infrared semiconductor broadband light emitters. *Light. Sci. & Appl.*, 7:17170, 2018.

[54] V. Mittal, G. Devitt, M. Nedeljkovic, L. G. Carpenter, H. M. H. Chong, J. S. Wilkinson, S. Mahajan, and G. Z. Mashanovich. Ge on Si waveguide mid-infrared absorption spectroscopy of proteins and their aggregates. *Biomed. Opt. Express*, 11(8):4714–4722, 2020.

[55] V. Vakarin, J. M. Ramírez, J. Frigerio, A. Ballabio, X. Le

Roux, Q. Liu, D. Bouville, L. Vivien, G. Isella, and D. Marris-Morini. Ultra-wideband Ge-rich silicon germanium integrated Mach–Zehnder interferometer for mid-infrared spectroscopy. *Opt. Lett.*, 42(17):3482–3485, 2017.

[56] V. Vakarin, J. M. Ramírez, J. Frigerio, Q. Liu, A. Ballaio, X. Le Roux, C. Alonso-Ramos, G. Isella, P. Cheben, W. N. Ye, L. Vivien, and D. Marris-Morini. Wideband Ge-rich SiGe polarization-insensitive waveguides for mid-infrared free-space communications. *Appl. Sci.*, 8(7):1154, 2018.

[57] Z. Cheng, X. Chen, C. Y. Wong, K. Xu, and H. K. Tsang. Mid-infrared suspended membrane waveguide and ring resonator on silicon-on-insulator. *IEEE Photonics J.*, 4(5):1510–1519, 2012.

[58] J. Soler Penadés, A. Ortega-Moñux, M. Nedeljkovic, J. G. Wangüemert-Pérez, R. Halir, A. Z. Khokhar, C. Alonso-Ramos, Z. Qu, Í. Molína-Fernández, P. Cheben, and G. Z. Mashanovich. Suspended silicon mid-infrared waveguide devices with subwavelength grating metamaterial cladding. *Opt. Express*, 24(20):22908–22916, 2016.

[59] J. Soler Penadés, A. Sánchez-Postigo, M. Nedeljkovic, J. G. Wangüemert-Pérez, Y. Xu, R. Halir, Z. Qu, A. Z. Khokhar, A. Osman, W. Cao, C. G. Littlejohns, P. Cheben, Í. Molína-Fernández, and G. Z. Mashanovich. Suspended silicon waveguides for long-wave infrared wavelengths. *Opt. Lett.*, 43(4):795–798, 2018.

[60] W. Zhou, Z. Cheng, X. Wu, X. Sun, and H. K. Tsang. Fully suspended waveguide platform. *J. Appl. Phys.*, 123(6):063103, 2018.

[61] T. T. D. Dinh, X. Le Roux, N. Koompai, D. Melati, M. Montesinons-Ballester, D. González-Andrade, P. Cheben, A. V. Velasco, E. Cassan, D. Marris-Morini, L. Vivien, and C. Alonso-Ramos. Mid-infrared Fourier-transform spectrometer based on metamaterial lateral cladding suspended silicon waveguides. *Opt. Lett.*, 47(4):810–813, 2022.

[62] A. Sánchez-Postigo, J. G. Wangüemert-Pérez, J. Soler Penadés, A. Ortega-Moñux, M. Nedeljkovic, R. Halir, F. El Mokhtari Mimun, Y. X. Cheng, Z. Qu, A. Z. Khokhar, A. Osman, W. Cao, C. G. Littlejohns, P. Cheben, G. Z. Mashanovich, and Í. Molína-Fernández. Mid-infrared suspended waveguide platform and building blocks. *IET Optoelectron.*, 13(2):55–61, 2019.

[63] C. G Littlejohns, D. J. Rowe, H. Du, K. Li, W. Zhang, W. Cao, T. Dominguez Bucio, X. Yan, M. Banakar, D. Tran, S. Liu, F. Meng, B. Chen, Y. Qi, X. Chen, M. Nedeljkovic, L. Mastronardi, R. Maharjan, S. Bohora, A. Dhakal, I. Crowe, A. Khurana, K. C. Balram, L. Zagaglia, F. Floris, P. O'Brien, E. Di Gaetano, H. M. H. Chong, F. Y. Gardes, D. J. Thomson, G. Z. Mashanovich, M. Sorel, and G. T. Reed. CORNERSTONE's silicon photonics rapid prototyping platforms: current status and future outlook. *Appl. Sci.*, 10(22):8201, 2020.

[64] W. Liu, Y. Ma, X. Liu, J. Zhou, C. Xu, B. Dong, and C. Lee. Larger-than-unity external optical field confinement enabled by metamaterial-assisted comb waveguide for ultrasensitive long-wave infrared gas spectroscopy. *Nano Lett.*, 22(15):6112–6120, 2022.

[65] F. Nikalaus, C. Vieider, and H. Jakobsen. MEMS-based uncooled infrared bolometer arrays: a review. *Proc. SPIE*, 6836, 2008.

[66] Y. Wu, Z. Qu, A. Osman, W. Cao, A. Z. Khokhar, J. Soler Penades, O. L. Muskens, G. Z. Mashanovich, and M. Nedeljkovic. Mid-infrared nanometallic antenna assisted silicon waveguide based bolometers. *ACS Photonics*, 6(12):3253–3260, 2019.

[67] Y. Wu, Z. Qu, A. Osman, C. Wei, W. Cao, A. Tarazona, S. Z. Oo, H. M. H. Chong, O. L. Muskens, G. Z. Mashanovich, and M. Nedeljkovic. Nanometallic antenna-assisted amorphous silicon waveguide integrated bolometer for mid infrared. *Opt. Lett.*, 46(3):677–680, 2021.

[68] G. Son, S. Han, J. Park, K. Kwon, and K. Yu. High-efficiency broadband light coupling between optical fibers and photonic integrated circuits. *Nanophotonics*, 7(12):1845–1864, 2018.

[69] N. Chen, B. Dong, X. Luo, H. Wang, N. Singh, G.-Q. Lo, and C. Lee. Efficient and broadband subwavelength grating coupler for 3.7 µm mid-infrared silicon photonics integration. *Opt. Express*, 16(20):26242–26256, 2018.

[70] Z. Cheng, X. Chen, C. Y. Wong, K. Xu, C. K. Y. Fung, Y. M. Chen, and H. K. Tsang. Mid-infrared grating couplers for silicon-on-sapphire waveguides. *IEEE Photonics J.*, 4(1):104–113, 2012.

[71] Z. Cheng, X. Chen, C. Y. Wong, K. Xu, C. K. Y. Fung, Y. M. Chen, and H. K. Tsang. Focusing subwavelength grating coupler for mid-infrared suspended membrane waveguide. *Opt. Lett.*, 37(7):1217–1219, 2012.

[72] J. Kang, Z. Cheng, W. Zhou, T.-H. Xiao, K.-L. Gopalakrisna, M. Takenaka, H. K. Tsang, and K. Goda. Focusing subwavelength grating coupler for mid-infrared suspended membrane germanium waveguides. *Opt. Lett.*, 42(11):2094–2097, 2017.

[73] R. Wang and Y. Wang. Fourier transform infrared spectroscopy in oral cancer diagnosis. *Int. J. Mol. Sci.*, 22(3):1206, 2021.

[74] D. J. Rowe, D. Smith, and J. S. Wilkinson. Complex refractive index spectra of whole blood and aqueous solutions of anticoagulants, analgesics and buffers in the mid-infrared. *Sci. Reports*, 7(7356), 2017.

[75] K. Bougot-Robin, J. P. Hugonin, M. Besbes, and H. Benisty. Broad working bandwidth and "endlessly" single-mode guidance within hybrid silicon photonics. *Opt. Lett.*, 40(15):3512–3515, 2015.

[76] C. J. Stirling, W. Cao, J. D. Reynolds, T. D. Bradley, L. Mastronardi, F. Y. Gardes, and M. Nedeljkovic. Mid-infrared silicon-on-insulator waveguides with single-mode propagation over an octave of frequency. *Opt. Express*, 30(6):8560–8570, 2022.

[77] R. Halir, P. Cheben, J. M. Luque-González, Jose Dario Sarmiento-Merenguel, J. H. Schmid, G. Wangüemert-Pérez, D.-X. Xu, S. Wang, A. Ortega-Moñux, and Í. Molína-Fernández. Ultra-broadband nanophotonic beamsplitter using an anisotropic sub-wavelength metamaterial. *Laser & Photonics Rev.*, 10(6):1039–1046, 2016.

[78] A. Maese-Novo, R. Halir, S. Romero-Garcí, D. Pérez-Galacho, L. Zavargo-Peche, A. Ortega-Moñux, Í. Molína-Fernández, J. G. Wangüemert-Pérez, and P. Cheben. Wavelength independent multimode interference coupler. *Opt. Express*, 21(6):7033–7040, 2013.

[79] C. J. Stirling, R. Halir, A. Sánchez-Postigo, Z. Qu, J. D. Reynolds, J. Soler Penadés, G. S. Murugan, A. Ortega-Moñux, J. G. Wangüemert-Pérez, Í. Molína-Fernández, G. Z. Mashanovich, and M. Nedeljkovic. Broadband 2×2 multimode interference coupler for mid-infrared wavelengths. *Opt. Lett.*, 46(21):5300–5303, 2021.

[80] T. Hu, M. S. Rouifed, H. Qiu, X. Guo, C. G. Littlejohns, C. Liu, and H. Wang. A polarization splitter and rotator based on a partially etched grating-assisted coupler. *IEEE Photonics Technol. Lett.*, 28(8):911–914, 2016.

[81] B. Dong, T. Hu, X. Luo, Y. Chang, X. Guo, H. Wang, D.-L. Kwong, G.-Q. Lo, and C. Lee. Wavelength-flattended directional coupler based mid-infrared chemical sensor using Bragg wavelength in subwavelength grating structure. *Nanomaterials*, 8(11):893, 2018.

[82] Z. Jafari and A. Zarifkar. Dispersion flattened single etch-step waveguide based on subwavelength grating. *Opt. Commun.*, 393:219–223, 2017.

[83] T. T. D. Dinh, J. Zhang, P. Nuño-Ruano, D. González Andrade, X. Le Roux, M. Montesinos Ballester, C. Lafforgue, D. Medina Quiroz, D. Benedikovic, P. Cheben, D. Bouville, N. D. Lanzillotti Kimura, D. Marris-Morini, E. Cassan, L. Vivien, and C. Alonso Ramos. Subwavlength silicon nanostructuration for nonlinear and optomechanic applications. *Proc. SPIE*, PC12425, 2023.

[84] D. Benedikovic, M. Berciano, C. Alonso-Ramos, X. Le Roux, E. Cassan, D. Marris-Morini, and L. Vivien. Dispersion control of silicon nanophotonic waveguides using sub-wavelength grating metamaterials in near- and mid-IR wavelengths. *Opt. Express*, 25(16):19468–19478, 2017.

[85] B. Szelag, S. Garcia, L. Adelmini, M. Kazar-Mendes, S. Guerber, S. Congia, A. Myko, P. Grosse, L. Virot, and Q. Wilmart.

High performance 300mm silicon photonics platform for R&D and product prototyping. *IEEE Photonics Conf.*, 2022.

[86] V. Vakarin, D. Melati, T. T. D. Dinh, X. Le Roux, W. K. K. Kan, C. Dupré, B. Szelag, S. Monfray, F. Boeuf, P. Cheben, E. Cassan, D. Marris-Morini, L. Vivien, and C. A. Alonso-Ramos. Metamaterial-engineered silicon beam splitter fabricated with deep UV immersion lithography. *Nanomaterials*, 11(11):2949, 2021.